Early-Season Crop Mapping on an Agricultural Area in Italy Using *X*-Band Dual-Polarization SAR Satellite Data and Convolutional Neural Networks

Giacomo Fontanelli ⓘ, Alessandro Lapini ⓘ, Leonardo Santurri ⓘ, Simone Pettinato ⓘ, *Member, IEEE*, Emanuele Santi ⓘ, *Senior Member, IEEE*, Giuliano Ramat ⓘ, Simone Pilia ⓘ, *Member, IEEE*, Fabrizio Baroni ⓘ, *Senior Member, IEEE*, Deodato Tapete ⓘ, Francesca Cigna ⓘ, and Simonetta Paloscia ⓘ, *Fellow, IEEE*

Abstract—Early-season crop mapping provides decision-makers with timely information on crop types and conditions that are crucial for agricultural management. Current satellite-based mapping solutions mainly rely on optical imagery, albeit limited by weather conditions. Very few exploit long-time series of polarized synthetic aperture radar (SAR) imagery. To address this gap, we assessed the performance of COSMO-SkyMed *X*-band dual-polarized (HH, VV) data in a test area in Ponte a Elsa (central Italy) in January–September 2020 and 2021. A deep learning convolutional neural network (CNN) classifier arranged with two different architectures (1-D and 3-D) was trained and used to recognize ten classes. Validation was undertaken with *in situ* measurements from regular field campaigns carried out during satellite overpasses over more than 100 plots each year. The 3-D classifier structure and the combination of HH+VV backscatter provide the best classification accuracy, especially during the first months of each year, i.e., 80% already in April 2020 and in May 2021. Overall accuracy above 90% is always marked from June using the 3-D classifier with HH, VV, and HH+VV backscatter. These experiments showcase the value of the developed SAR-based early-season crop mapping approach. The influence of vegetation phenology, structure, density, biomass, and turgor on the CNN classifier using *X*-band data requires further investigations, along with the relatively low producer accuracy marked by vineyard and uncultivated fields.

Index Terms—Convolutional neural network (CNN), COSMO-SkyMed, crop early mapping, deep learning, dual polarization, synthetic aperture radar (SAR), *X*-band.

I. INTRODUCTION

MODERN agriculture will have to combine the needs of productivity with those of environmental, economic, and social sustainability [1] in a climatic context made uncertain by the effects of climate change [2]. Information that can help in implementing advanced and integrated monitoring and forecasting systems to promptly identify the risks and the impacts of calamities and crop practices on agricultural environments is essential. Satellite Earth observation data were revealed to be optimal for the aforementioned tasks for three main reasons.

1) From the spatial point of view, they can cover wide areas with different spatial resolutions [3].
2) From the temporal point of view, since they can be frequent, they can benefit from historical series for long-term analysis [4], and they can be punctual thanks to the continuous acquisition of Copernicus constellations [5].
3) From an economic point of view, they are becoming more convenient thanks to the provision of free satellite data and software for their processing and display [6], [7].

Agricultural ecosystems are characterized by strong variations within relatively short time intervals. Depending on the observation period, the agricultural scenario can present itself in a totally different way due to the different biomass, phenology, and turgor that can be driven by cultivar and agricultural working, as well as weather conditions. These dynamics are challenging for crop classification and the knowledge of vegetation status can deliver crucial information that can be used to improve the classifier's performance [8].

To consider these aforementioned changes in agricultural vegetation and soil status, a multitemporal approach based on the study of time series of remotely sensed indices was revealed to be successful [9], [10]. Time series of satellite images offer the opportunity to retrieve the dynamic properties of target surfaces by investigating their spectral properties combined with temporal information on their changes [11].

Crop mapping represents important information in the context of programs for the monitoring of rural areas on a regional and global scale [12], [13].

Giacomo Fontanelli, Alessandro Lapini, Leonardo Santurri, Simone Pettinato, Emanuele Santi, Giuliano Ramat, Simone Pilia, Fabrizio Baroni, and Simonetta Paloscia are with the Institute of Applied Physics N. Carrara, National Research Council, 50019 Florence, Italy (e-mail: g.fontanelli@ifac.cnr.it; a.lapini@ifac.cnr.it; l.santrurri@ifac.cnr.it; s.pettinato@ifac.cnr.it; e.santi@ifac.cnr.it; g.ramat@ifac.cnr.it; s.pilia@ifac.cnr.it; f.baroni@ifac.cnr.it; s.paloscia@ifac.cnr.it).

Deodato Tapete is with the Italian Space Agency, 00133 Rome, Italy (e-mail: deodato.tapete@asi.it).

Francesca Cigna was with the Italian Space Agency, 00133 Rome, Italy. She is now with the Institute of Atmospheric Sciences and Climate, National Research Council, 00133 Rome, Italy (e-mail: f.cigna@isac.cnr.it).

Digital Object Identifier 10.1109/JSTARS.2022.3198475

The early season mapping (ESM) allows for a refinement of crop mapping and plays a prominent role in facilitating the following:

1) the prediction of water consumption due to irrigation in water balance monitoring [14], [15];
2) the control of pesticides [16];
3) the control of food production and waste [17];
4) the control of many prescriptions is contained in the plans of the Community Economic Policy.

ESM is also the basis for developing algorithms and systems for monitoring the growth of vegetation and for the estimation of biomass and yield [18]. The main aim of ESM is therefore to provide public and private decision-makers with timely information on crop types and conditions that are revealed to be crucial for agricultural management in the context of programs for rural areas and resource management on a regional and global scale [19], [20]. ESM is based on the recognition of incomplete series of temporal trends of optical or microwave indices; more in detail ESM is carried out using only remotely sensed data acquired in the first months of the agricultural years. The quality of classification and the time horizon in which crop maps can be provided depends on the type and temporal resolution of satellite data, the classifier, and the operator's ability.

In literature, many studies showed the effectiveness of satellite optical data for crop mapping with moderate [21], [22], high [23], [24], very high resolution products [25], [26], and with their fusion [27], [28], using the bands or arranging them in optical indices [29], [30], with object- or pixel-based approaches [31], [32]. However, the usability of optical satellite data is strongly hampered by illumination and weather conditions since they can acquire images only in daytime and in cloud-free sky states. On the contrary, microwave sensors are generally not affected by weather conditions, clouds, and sun illumination, and with the advent and the evolution of synthetic aperture radar (SAR) sensors, the geometric resolution of the imagery is becoming even closer to the optical one.

Several studies describe crop mapping results carried out using *L*- [33], [34], *C*- [35], [36], and *X*-band [37], [38] over the integration of multifrequency sensors [33], [39]. Polarimetric SAR data and the related polarimetric-SAR technology were revealed to be breakthroughs for classification since they can benefit from up to four polarizations and a set of different decomposition algorithms that can derive new features from the whole scattering matrix to be used by the classifiers [40], [41].

The dual-polarization *X*-band SAR data showed good performances in mapping and monitoring the phenology of agricultural environments, both with TerraSAR-X data [42], [43] and COSMO-SkyMed StripMap imagery [44], [45].

Machine learning techniques have been applied in crop mapping with satellite data, for example, using support vector machines [46], [47], random forest [48], [49], or artificial neural networks [12], [50]. Deep learning (DL) is a subset of machine learning based on artificial neural networks related with an unbounded number of layers of bounded size, permitted to be heterogeneous and to deviate widely from biologically informed connectionist models [51]. The performances demonstrated by

DL approaches in many areas of image processing have generated considerable interest in the extension of DL techniques to the entire universe of remote sensing, including features extraction [52], change-detection [53], and data fusion [54].

DL techniques were used for classification exploiting optical imagery with subdecimeter resolution [55], [56], very high spatial resolution [57], [58], hyperspectral [59], [60], and multispectral satellite data [61], [62]. SAR image classification using DL was described in [63], with polarimetric data in [64] and [65] and in integration with optical data in [66]. Ensemble and DL techniques have been proved to outperform other machine learning techniques such as support vector machines [67], [68] since they take advantage of the redundancy in the number of classifiers to decrease the variance of the estimation error.

Crop mapping is another important task that can benefit from the application of DL techniques with optical [69], [70] and the fusion/integration of optical and SAR data [66], [71], [72]. Few manuscripts describe the results from the use of DL techniques with SAR imagery for land and crop classification [73], [74], despite the good classification accuracy and efficiency [75]. In [76], Hirose used DL to conduct several pioneering works on land use classification with SAR.

A convolutional neural network (CNN) is a class of DL able to learn high-level context features through a large number of neurons arranged in multiple architectures. Especially, 3-D convolution can take into account the radiometric, spatial, and temporal components of a multitemporal stack of satellite scenes in a more delicate and rigorous manner, other than a direct concatenation of reflectance or backscatter images [77]. The main flaw in the use of CNN is represented by the high number of samples required during the training.

The present study evaluates the performance of CNN applied to in-season early crop classification of an agricultural area in the center of Tuscany, Italy, during 2020–2021. The test area is interesting for crop classification due to the small dimension of the fields and the similarity in life cycles of some crops that can be easily confused by the classifiers. *X*-band satellite data, purposely tasked and collected by means of the Italian Space Agency (ASI)'s COSMO-SkyMed constellation in StripMap PingPong mode, were used. The novelty of this work lies on 1) the use of *X*-band SAR backscatter alone for early crop mapping, in particular exploiting an unprecedentedly long and continuous time series of dual-polarization data; and 2) the analysis of the marginal gain obtained by postponing the production date of the classified map, which technically consists of an increase in the available satellite SAR scenes used for classification. Several tests were done to identify and assess the best CNN architecture, the different performance of the classifiers depending on the time of maps delivery, and the difference in accuracy attained using single-polarization versus dual-copolarized data.

II. MATERIALS AND METHODS

A. Test Site and Ground Data

The selected test site extends 270 ha and is located south of Ponte a Elsa (43°41′20.37″N, 10°53′42.38″E), a small town in
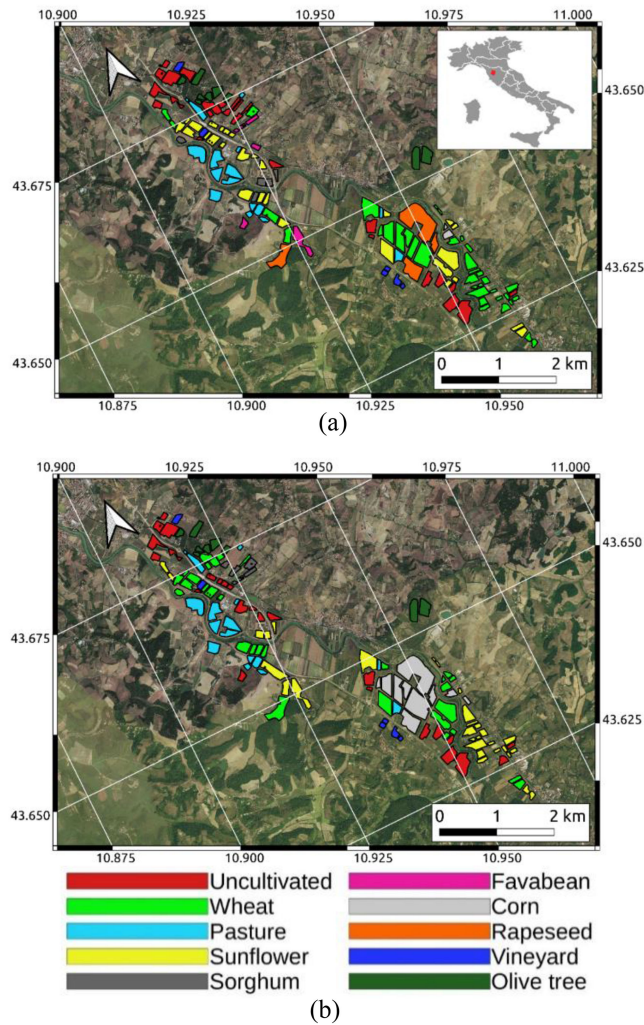
Fig. 1. Map of investigated fields in the Ponte a Elsa test site in (a) 2020 and (b) 2021.

TABLE I
ACQUISITION DATES OF COSMO-SKYMED STRIPMAP PINGPONG PRODUCTS
IN 2020 AND 2021 OVER THE PONTE A ELSA TEST SITE

Year 2020		Year 2021	
Date	DOY	Date	DOY
11/01/2020	11	13/01/2021	13
27/01/2020	27	14/02/2021	45
12/02/2020	43	02/03/2021	61
28/02/2020	59	03/04/2021	93
15/03/2020	75	19/04/2021	109
31/03/2020	91	01/05/2021	121
16/04/2020	107	05/05/2021	125
02/05/2020	123	21/05/2021	141
18/05/2020	139	29/05/2021	149
03/06/2020	155	02/06/2021	153
01/07/2020	183	06/06/2021	157
21/07/2020	203	04/07/2021	185
29/07/2020	211	08/07/2021	189
22/08/2020	235	05/08/2021	217
		09/08/2021	221

fava bean) and summer crops (sorghum, corn, and sunflower) that follow the annual field's rotation. Vineyard, olive tree, and pasture can be considered multiyear crops.

Winter species are generally seeded in autumn before the year of harvesting, i.e., wheat harvested in mid-June 2020 was seeded approximately in October 2019. Summer species are seeded the same year of harvesting, i.e., the sunflower harvested at the end of August 2021 was seeded approximately in April 2021. Pasture class consists mainly of forage crops, like alfalfa, clover, cat grass, oat, fennel, etc. These plots are grazed many times in a year. Finally, the uncultivated class is represented by natural vegetation that invades the fields during the year of rest from agricultural cultivation.

B. Satellite Synthetic Aperture Radar (SAR) Data

X-band SAR data from the COSMO-SkyMed (CSK) constellation [79] were collected for this research by ASI during a tailored monitoring campaign designed in 2019 and carried out in the framework of the project "ALGORITMI" [80].

StripMap PingPong (CSK-PP) images were acquired in right-looking mode along ascending orbits (at ∼05:00 A.M. UTC), using alternating polarization HH and VV. The beam mode PP_12 was used, with an off-nadir angle ranging between 37.9° (near range) and 39.7° (far range) and an incidence angle between 42.6° and 44.4°, respectively. Following two periods of acquisitions were selected for the analysis: 1) from 1st January 2020 till 31st August 2020 and 2) from 1st January 2021 till 31st August 2021. Dates of imagery are provided in Table I.

CSK-PP scenes were accessed as single-look complex slant range products (Level 1A), then multilooked to obtain squared pixel maps. The Ponte a Elsa test site lies on a flat plain, and thus, its backscatter is not influenced by orography. Anyway, terrain correction has been applied considering the formulas

the Tuscany region, Italy, divided between the municipalities of Empoli (Florence) and San Miniato (Pisa), as shown in Fig. 1.

The area is mainly suited to viticulture and olive growing, and annual herbaceous crops like maize, sunflower, sorghum, wheat, and legumes are a secondary source of income for the small local farms, which generally do not exceed a few tens of hectares. The selected agricultural plots belong to five different farms and are located on the plain along the Elsa riverbed, surrounded by low and mild hills. Selected plots are always bigger than 1 ha with an average of approximately 3 ha. They have an irregular shape and are delimited by moats or shrubs. A criterion for the selection of those fields was the homogeneity in terms of species, soil type, and cultivation.

The plots were surveyed during several measurement campaigns carried out in spring 2020 and 2021 using the SMASH Field Data Collection mobile application [78], which allows the collection of georeferenced pictures with notes attached that can easily be exported in any vector format.

Herbaceous crops in the Ponte a Elsa test site are always annual and can be grouped in winter (wheat, rapeseed, and
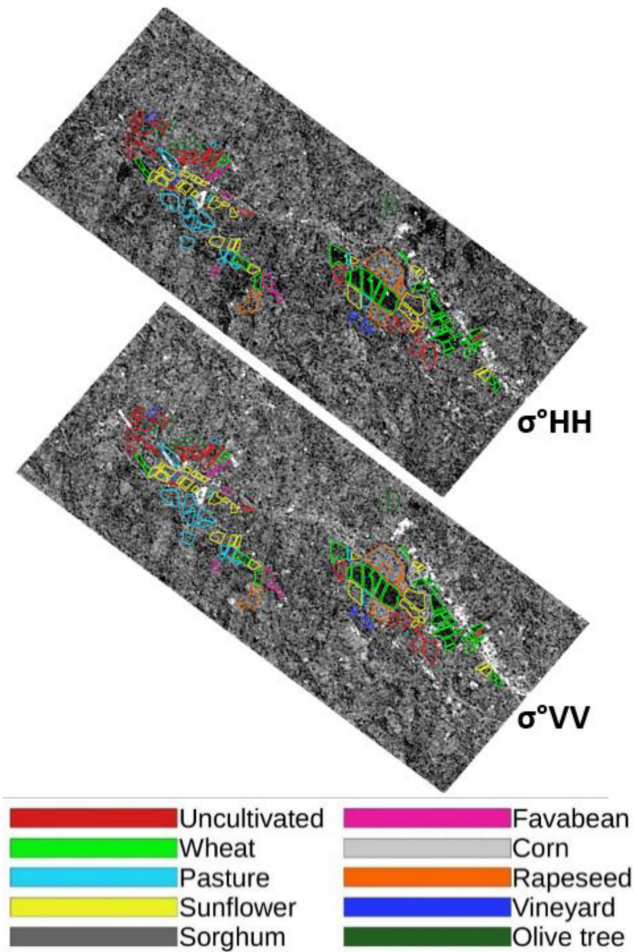
Fig. 2. Example of *X*-band COSMO-SkyMed StripMap PingPong sigma naught in HH and VV polarization acquired over the Ponte a Elsa test site on June 3, 2020 along with borders of test fields.

TABLE II
CLASS REPRESENTATIVENESS EXPRESSED AS NUMBER OF PLOTS AND NUMBER OF PIXELS PER CROP CLASS USED FOR THE EXPERIMENT IN 2020 AND 2021

Class	2020		2021	
	Number of plots	Number of pixels	Number of plots	Number of pixels
Sunflower	28	5904	30	5569
Sorghum	5	718	6	801
Corn	2	242	10	6797
Wheat	36	7904	30	6885
Favabean	6	1151	0	0
Rapeseed	4	4227	0	0
Uncultivated	26	5785	25	5453
Pastures	16	3965	16	3965
Vineyard	6	693	6	693
Olive	9	2141	9	2141

described in [81] and [82], using the 10-m resolution digital elevation model provided by Regione Toscana [83]. As a result, backscatter maps with a pixel dimension of 10 m, with the produced UTM 32N (EPSG 32632) projection, and are finally despeckled by means of a Kuan filter (window size $= 3 \times 3$ pixels, equivalent number of looks $= 1$).

CSK-PP products exploit an incoherent dual-polarization mode since the phase link between two polarimetric acquisitions is not preserved [84]. While this prevents the possibility of obtaining useful polarimetric features like alpha and entropy from a dual-polarization decomposition, as those derived in [43] and [85] using TerraSAR-X, this dataset provides sigma naught backscatter maps in both VV and HH polarization (as those shown in Fig. 2), which was the key parameter used in the research.

C. Classification Algorithm

Since the classifier is trained to recognize crops on the basis (especially) of temporal trends of backscatter and species from winter classes tend to have similar yearly backscatter temporal trends (the same for species from summer classes), this represents the first difficulty for classification. In this research, the differences in temporal trends inside crops from the winter macroclass (or summer macroclass) are led mainly by the amount of biomass per square meter, plant water content, and by the different structures of the plants [86].

The inclusion of uncultivated (fallow) and pasture classes acts as another burden for classification due to its high heterogeneity in biomass, floristic composition, and dates of grazing or harvesting.

Furthermore, the entire 2020 and 2021 ground truth datasets were strongly unbalanced in terms of the number of pixels per class for both years as shown in Table II, although the variability of crops from one year to another depends on farmers' practice and decisions that cannot always be predictable.

On the other side, efforts were made to ensure a robust field data sample to cover each crop class through as many regular field visits as they were possibly allowed during a period of pandemic emergency and related health protection measures.

Eight following time steps were selected for the research, namely February, March, April, May, June, July, August, and September. For example, classification carried out in August consisted in producing a crop map feeding a classifier with a time series of SAR images spanning from January to July.

This article is focused on ensemble classifiers based on CNNs to perform crop classification over multitemporal CSK-PP imagery. An ensemble classifier is composed of three independently trained CNN classifiers. For a given input, the CNN classifiers produce a similarity score for each possible output class; the ensemble classifier output corresponds to the class that has the highest cumulative similarity score. Each CNN classifier operates on an input feature vector and provides a corresponding class as output. The input feature vectors are defined starting from the multitemporal image stack depicted in Fig. 3, where the acquisitions are preliminarily coregistered and sorted by polarizations (fast variable) and acquisition dates (slow variable).

In this experiment, the comparison of two CNN architectures that work on different kinds of input feature vectors as described
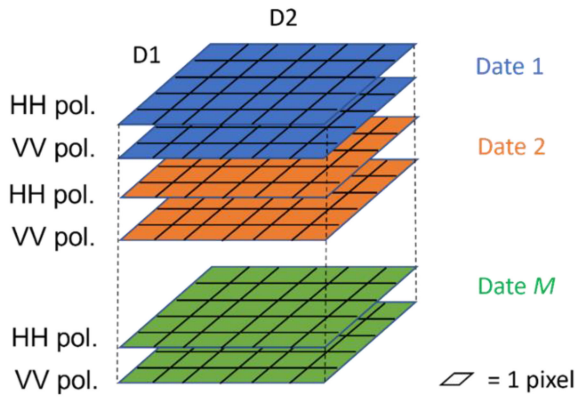
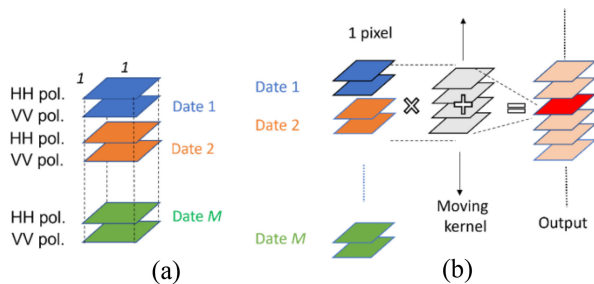Fig. 3. Generic image stack for the considered classification algorithms.

Fig. 4. 1-D CNN. (a) Input feature vector. (b) Convolution in the polarization time domain.

Fig. 5. 3-D CNN. (a) Input feature vector. (b) Convolution in the space+time domain.

TABLE III
PARAMETERS SETTING OF THE COMPARED CNN ARCHITECTURES

Architecture	Convolutional layer: kernel size	Convolutional layer: number of filters	Max pooling size	Dropout probability	First fully connected output size
1D-CNN	9,7,5,3	64, 128, 256, 512	2,2,2,2	20%	70,80,90
3D-CNN	[2,2,9], [1,1,7], [1,1,5], [1,1,3]	64, 128, 256, 512	[2,2,2], [1,1,2], [1,1,2], [1,1,2]	20%	70,80,90

in [66], i.e., one-dimensional and three-dimensional (hereafter abbreviated as 1-D and 3-D), was done. The former is called 1-D because the convolution kernel is single-dimensional and operates in the vectorized polarization-time domain, as shown in Fig. 4. In the latter, the input feature vectors are patches of size 3-by-3 pixels [see Fig. 5(a)], and the convolutional kernels span the polarizations and operate in the 3-D domain defined by the space and the time coordinates, as shown in Fig. 5(b). Both the architectures provide pixel-by-pixel classification.

In the case of 1-D, this behavior is implicitly given by the size of the input feature vector; for the 3-D, this is accomplished by considering a 3-by-3 patch centered on each image pixel and assigning to it the classification output. The patch dimension, both for 1-D and 3-D classifiers, is a tradeoff between limiting the misclassification along the parcels' borders and grasping the contextual features.

The parameter values adopted in the previous layers are listed in Table III. The convolutional layer is responsible for linearly filtering the input to extract the features for the subsequent layers.

The batch normalization layer is introduced to stabilize the training process making it less dependent on the values of each minibatch in the learning phase. The rectifier linear unit (ReLu) layer is a common choice in the supervised classification of images [66] due to its efficient implementation and plausibility with the underlying signal model. The role of the max pooling layer is to reduce the number of outputs at each stage by preserving the local maxima of its input.

Independent of the architecture, the CNN classifiers of an ensemble share the following multilayer structure:
1) input layer;
2) four *convolutional* blocks;
3) first fully connected layer;
4) second fully connected layer;
5) softMax layer;
Each convolutional block is composed of the following:
1) convolutional layer;
2) batch normalization layer;
3) ReLu activation function;
4) max pooling layer;
5) dropout layer.
The dropout layer aims at reducing the overfitting by ignoring some of its inputs randomly chosen. The fully connected layers synthesize the output of the convolutional blocks by interconnecting all their inputs. Finally, the softmax layer provides the similarity score for each of the possible output classes. It is necessary to remark that the structure of the CNN classifiers in an ensemble classifier is the same, being the output size of

the first fully connected layer the only difference (see the last column of Table III); this setting has been successfully adopted also in [66] and [87].

The training of the CNN classifiers is performed by means of the adaptive moment estimation algorithm [88], which is a common choice for this kind of problem. The minibatch size and the number of epochs are set to 128 and 100, respectively, with shuffling at the end of each epoch to reduce the overfitting. The initial learning rate is set to 10^{-3} with a dropping factor of 0.1 every 20 epochs; the cross entropy with L_2 regularization is used as a loss function to avoid divergent behavior. A stratified threefold partitioning of the dataset was used in all experiments. In turn, two partitions are first oversampled by means of Synthetic Minority Oversampling Technique plus Tomek Links (SMOTE+TL), [88] to deal with the dataset unbalancing and then used to train an ensemble classifier from scratch; the remaining partition is used for testing. The presented results and related statistics are computed over the union of the testing partitions.

III. RESULTS

The results of early crop mapping using CSK-PP data and CNN for 2020 and 2021 are shown in Tables IV and V. Two metrics are used to describe the goodness of classification in this article, namely overall accuracy (OA) and producer accuracy (PA). The former is defined as the ratio of the number of correctly classified pixels over its total number; the latter is defined as the number of pixels correctly classified to a specific class over the total number of pixels of that class.

A. Achieved Classification Performance in Terms of OA

In 2020, two big increases are found in OA of crop classification in March (32.5%) and in April (almost 25%) when using 1-D with the combination of HH and VV (hereafter called 1D-HH+VV), when two and four SAR images, respectively, were available. Using a 3-D classifier, the highest increase in OA happens in March, with a difference above 33% using HH or VV (these combinations will be called, respectively, 3D-HH and 3D-VV hereafter) and above 31% using HH+VV (hereafter called 3D-HH+VV).

In 2021, a big increase was found in OA, above 30% in June using backscatter from only HH or VV and 1-D (these combinations will be called, respectively, 1D-HH and 1D-VV hereafter). For 1D-HH+VV this increase is approximately 27% and occurs earlier, i.e., in May, when ten and six images are respectively available. Using a 3-D classifier, the boost in classification performance is immediately higher over time with respect to 1-D until June. With 3D-HH+VV the highest increase of OA over time happens in March and is above 30%, achieved using only two SAR images. With 3D-HH and 3D-VV, the highest increase of OA occurs later, i.e., in June.

In 2020, VV was found slightly more semantic for crop classification with respect to HH from March, with an average gap of approximately 2% for 1-D. HH+VV always provides better classification performance with respect to the use of backscatter from a single polarization, with both 1-D and 3-D.

TABLE IV
OA OF CROP CLASSIFICATION OF PONTE A ELSA TEST SITE ATTAINED IN EIGHT MONTHLY TIME STEPS IN 2020 WITH TWO CNN: 1-D AND 3-D AND BACKSCATTER FROM COSMO-SKYMED STRIPMAP PINGPONG DATA IN HH, VV, AND HH+VV

	Metric %	1D			3D		
		HH	VV	HH+VV	HH	VV	HH+VV
Feb	OA	16.5	16.5	24.2	25.5	26.5	46.5
	min PA (crop)	1.9 SF	2.3 SF	11.1 SF	12.3 WH	13.7 WH	31.5 WH
	max PA (crop)	59.5 CR	49.2 SR	59.9 CR	73.6 CR	62.0 CR	87.6 CR
Mar	OA	29.5	29.4	56.7	59.7	60.0	78.2
	min PA (crop)	17.7 SF	14.9 SF	46.9 SF	48.4 WH	51.5 UN	72.2 UN
	max PA (crop)	70.2 CR	74.1 SR	85.2 SR	93.0 CR	87.6 CR	95.0 CR
Apr	OA	46.1	48.1	81.6	75.0	76.2	89.0
	min PA (crop)	33.3 UN	35.1 UN	75.3 UN	68.6 UN	64.6 UN	84.0 UN
	max PA (crop)	78.1 CR	73.6 CR	91.8 SR	95.0 CR	95.5 CR	97.9 CR
May	OA	53.7	55.2	86.8	85.9	86.2	94.9
	min PA (crop)	39.9 SF	41.2 UN	80.8 UN	82.6 UN	81.5 UN	93.2 VN
	max PA (crop)	80.2 CR	78.7 SR	94.6 CR	95.9 CR	95.1 SR	97.9 CR
Jun	OA	72.1	74.4	94.3	95.8	95.9	98.5
	min PA (crop)	58.2 UN	62.1 UN	91.0 UN	92.9 VN	93.1 VN	96.0 VN
	max PA (crop)	87.6 CR	87.2 SR	96.2 SR	97.5 CR	97.9 WH	99.0 RS
Jul	OA	76.2	79.1	95.5	96.3	96.8	98.8
	min PA (crop)	63.7 UN	68.6 UN	92.9 VN	93.5 VN	92.4 VN	95.7 VN
	max PA (crop)	89.3 CR	89.8 SR	97.1 CR	97.5 WH	98.3 WH	99.2 WH
Aug	OA	88.2	90.2	97.9	98.4	98.7	99.3
	min PA (crop)	80.9 UN	82.9 UN	96.2 VN	95.4 VN	96.1 VN	97.5 VN
	max PA (crop)	94.4 SR	94.7 RS	98.8 RS	99.3 RS	99.4 WH	99.6 WH
Sep	OA %	90.7	92.1	98.2	98.5	98.8	99.4
	min PA (crop)	84.5 UN	87.2 UN	96.8 VN	95.7 VN	97.3 VN	98.7 VN
	max PA (crop)	96.0 SR	95.2 RS	99.0 RS	99.1 RS	99.4 WH	99.7 SR

The advantage of HH+VV increases until April with 1-D, when a difference above 30% OA is noticeable with respect to using backscatter from one polarization only. In the case of 3-D, the highest difference in OA of classification attained using 3D-HH+VV is already noticeable in February, with a better performance of approximately 20% with respect to classification carried out using 3D-VV or 3D-HH. 3D-HH+HV provides the best classification results for both years, as shown in Tables IV and VI, and Figs. 6 and 8(a).

In 2021, classification using 1D-HH provides the worst results among all the tests, as shown in Tables V and VII and Figs. 7 and 8(b). The superiority of OA attained with 1D-VV with respect to 1D-HH increases until June and is almost always above 5%.

(a)

(b)

Fig. 6. (a) Comparison between ground truth map of Ponte a Elsa test site in 2020 produced using *in situ* campaigns and (b) result of classification with 3-D structure CNN-based classifier using COSMO-SkyMed StripMap PingPong HH and VV polarization backscatter at the end of the season.
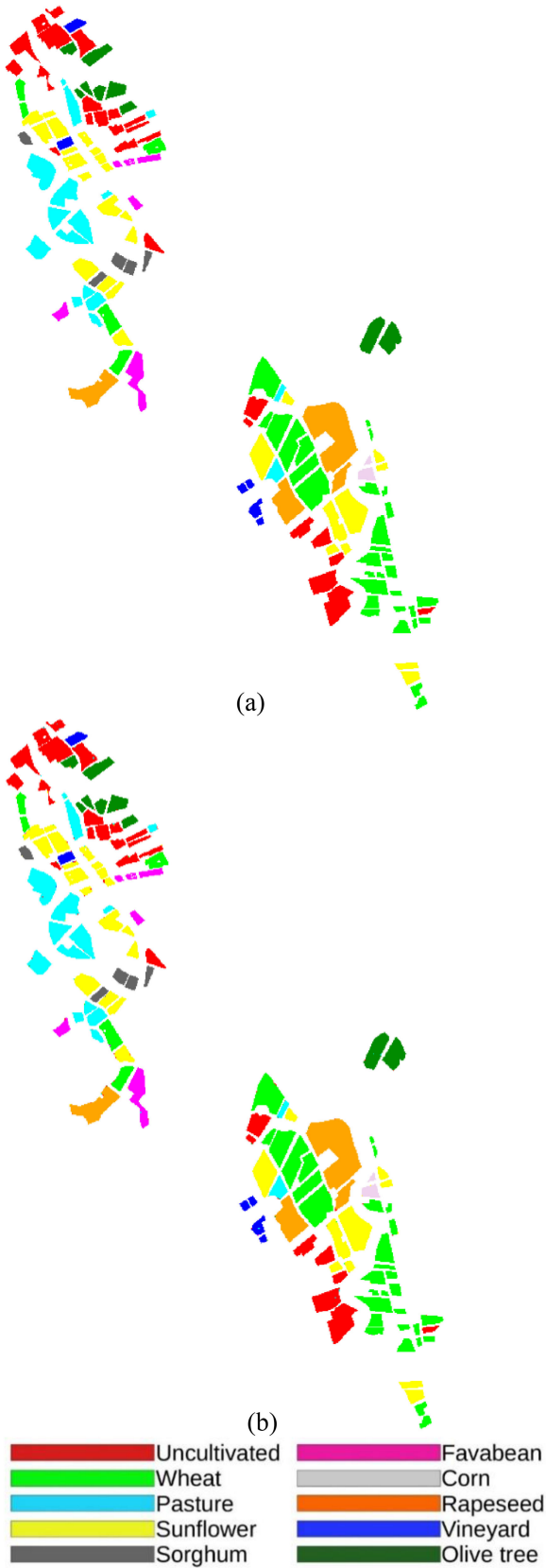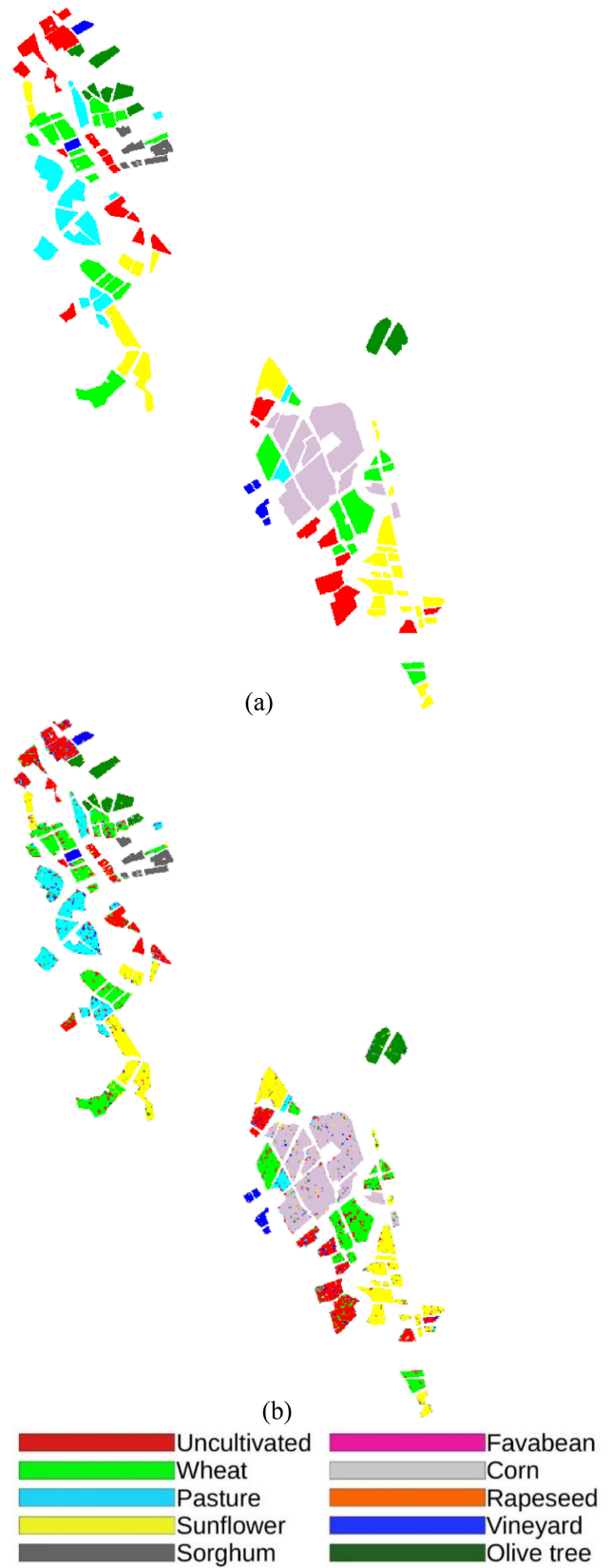

(a)

(b)

Fig. 7. (a) Comparison between ground truth map of Ponte a Elsa test site in 2021 produced using *in situ* campaigns and (b) result of classification with 1-D structure CNN-based classifier using COSMO-SkyMed StripMap PingPong HH polarization backscatter at the end of the season.

TABLE V
OA of Crop Classification of Ponte a Elsa Test Site Attained in Eight Monthly Time Steps in 2021 With Two CNN: 1-D and 3-D and Backscatter From COSMO-SkyMed StripMap PingPong Data in HH, VV, and HH+VV

	Metric %	1D			3D		
		HH	VV	HH+VV	HH	VV	HH+VV
Feb	OA	10.3	17.7	15.5	9.9	9.6	19.5
	min PA (crop)	0.0 UN	0.0 UN	0.1 UN	4.0 CR	2.6 WH	9.9 WH
	max PA (crop)	68.5 SR	48.9 PS	61.9 VN	36.8 SR	38.0 SR	41.8 SR
Mar	OA	15.2	20.2	27.3	30.6	30.9	49.8
	min PA (crop)	1.0 UN	0.0 UN	7.9 UN	17.2 UN	16.1 UN	36.7 UN
	max PA (crop)	70.0 SR	65.3 OT	68.7 OT	62.4 SR	55.1 SR	75.2 SR
Apr	OA	18.9	25.9	45.2	52.8	54.5	72.3
	min PA (crop)	3.6 UN	3.3 UN	28.0 UN	40.0 UN	41.9 CR	64.7 CR
	max PA (crop)	69.6 VN	65.2 OT	80.6 OT	83.6 SR	83.1 VN	90.8 SR
May	OA	36.4	44.4	72.2	67.8	71.5	83.8
	min PA (crop)	17.3 CR	15.4 UN	59.4 UN	57.3 UN	60.3 CR	76.5 WH
	max PA (crop)	72.7 SR	71.6 OT	89.6 OT	92.6 SR	89.9 VN	94.8 VN
Jun	OA	66.7	75.0	92.8	95.3	96.0	98.5
	min PA (crop)	52.4 UN	58.0 UN	89.2 UN	92.3 UN	93.7 UN	97.1 VN
	max PA (crop)	86.0 SR	87.2 OT	97.3 OT	98.3 SR	97.9 CR	99.0 CR
Jul	OA	76.3	82.7	95.6	97.1	97.4	99.0
	min PA (crop)	65.1 UN	70.9 UN	93.4 UN	94.2 VN	95.9 UN	97.3 VN
	max PA (crop)	92.4 SR	91.4 WH	98.5 OT	98.3 SR	98.1 CR	99.4 CR
Aug	OA	82.4	88.0	97.0	98.1	98.3	99.3
	min PA (crop)	73.5 UN	80.1 UN	95.0 UN	95.8 VN	97.0 VN	97.8 VN
	max PA (crop)	94.3 SR	92.7 OT	98.8 CR	98.6 CR	98.8 WH	96.0 CR
Sep	OA	87.6	92.0	98.0	98.5	98.8	99.5
	min PA (crop)	81.9 UN	85.5 UN	97.3 WH	94.8 VN	97.5 VN	98.3 VN
	max PA (crop)	95.4 SR	95.1 CR	99.2 CR	99.0 CR	99.2 WH	99.7 CR

TABLE VI
Confusion Matrix Relative to Classification Carried Out in 2020 Using 3-D Structure CNN-Based Classifier and COSMO-SkyMed StripMap PingPong HH+VV Polarization Backscatter

	FB	SF	WH	UN	CR	PS	SR	VN	OT	RS
FB	**1145**	1	0	3	0	2	0	0	0	0
SF	1	**5865**	5	21	1	4	1	2	1	3
WH	5	9	**7873**	12	0	4	0	0	1	0
UN	0	9	3	**5739**	0	23	1	0	7	3
CR	0	3	0	0	**239**	0	0	0	0	0
PS	0	2	3	13	0	**3941**	0	2	4	0
SR	0	1	0	0	1	0	**716**	0	0	0
VN	1	0	2	2	0	3	0	**684**	0	0
OT	0	1	0	6	0	3	0	0	**2129**	2
RS	1	4	0	10	0	1	0	0	3	**4208**

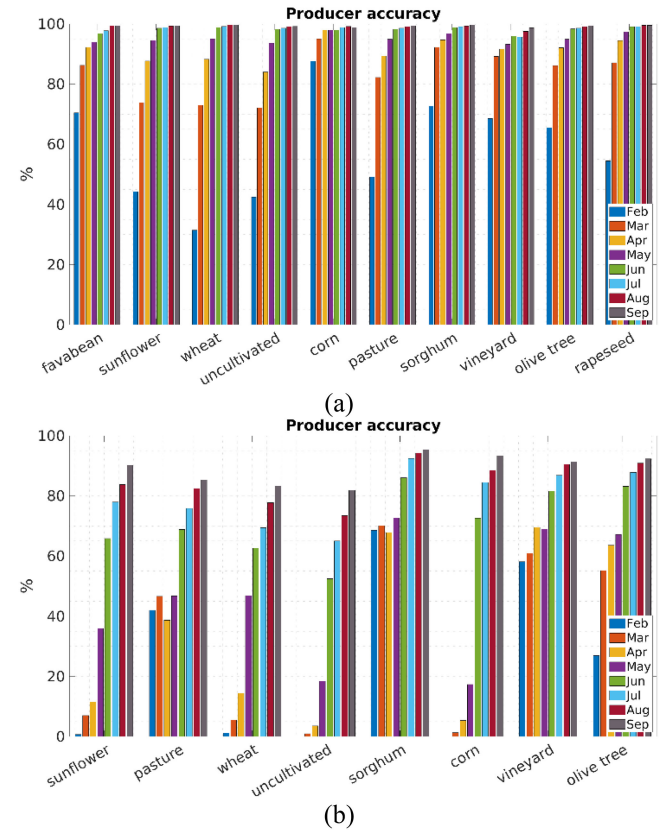The bold numbers highlight the correctly classified pixels for each crop class.

Fig. 8. Two examples of PA attained during the two years experiment with *X*-band backscatter and CNN-based classifier. (a) Best result attained with a 3-D structure of classifier and COSMO-SkyMed StripMap PingPong HH plus VV polarization backscatter in 2020. (b) Worst result attained with a 1-D structure of classifier and COSMO-SkyMed StripMap PingPong HH polarization backscatter in 2021.

Using 3-D, the difference in OA between classifications carried out using only HH or VV can be negligible, apart from April and May. In 2021, HH+VV allows the best OA to be achieved in crop classification when the advantage of using backscatter from both the polarizations increases until May using 1D-HH+VV. In this case, a difference of 35% of OA is noticeable with respect to using 1D-HH and above 25% using 1D-VV.

In the case of 3-D, a big difference in classification between using backscatter from both polarizations or a single one is noticeable already in March and April, with a better performance of approximately 20% of OA attained with respect to classification carried out using 1D-VV or 1D-HH. The difference in OA using HH+VV versus HH or VV drops dramatically after May using both 1-D and 3-D.

The OA in classification attained in 2020 is generally higher than the one in 2021, with the biggest difference reached in March or April. This is found although ten classes were required to be recognized in 2020 and eight in 2021. This assertion is valid generally until June when nine images were available in the 2020 dataset and ten in 2021. In this month, crop classification in 2020

	SF	PS	WH	UN	SR	CR	VN	OT
SF	**5019**	22	38	87	61	212	36	94
PS	21	**3381**	39	292	4	46	143	39
WH	134	115	**5705**	675	50	77	69	30
UN	69	234	243	**4465**	34	129	205	74
SR	4	3	4	6	**764**	14	0	6
CR	82	46	21	98	83	**6343**	59	65
VN	7	6	5	20	2	17	**633**	3
OT	40	10	1	30	21	50	12	**1977**

The bold numbers highlight the correctly classified pixels for each crop class.

and 2021 begins to attain the same OA with all polarizations, both for 1-D and 3-D, respectively.

B. Achieved Classification Performance in Terms of PA

The analysis of PA attained in the classification of crop types can help in the explanation of OA for each time frame, backscatter polarization, and CNN configuration. We first notice that all the tested classifiers exhibit a consistent behavior since the PAs in all classes improve and get closer as the deadline of the observation is postponed. Hence, increment in the OA is due to an improvement in all classes and not to improvements in the most represented classes only.

In 2020, sunflower, wheat, and, also, vineyard are the worst recognized classes at the beginning of the season. Uncultivated is a class that is easily confused especially at mid-season, along with vineyard at the end. The classes that are more recognizable are generally corn and sorghum and then wheat and rapeseed at the end of the season. PA of all the classes exceeds 90% late in the season, except for vineyard and uncultivated with 1D-HH and 1D-VV. In 2020 PA generally exceeds 90% just in June using 1D-HH+VV and 3-D with all the combinations of polarizations. The class that earlier exceeds or gets close to 90% of PA (just from March) is corn. Using 1D-HH and 1D-VV, the highest increment in PA is generally attained in June while using 1D-HH+VV and 3-D, this increase generally occurs earlier, i.e., in March, especially for corn, sorghum, pasture, vineyard, and olive tree. The increase in PA gained moving from HH or VV to HH+VV with 3-D is more limited. Moving from 1-D to 3-D, a noticeable amelioration in PA of all the classes is noticeable, especially for wheat.

In 2021, the worst recognized class at the beginning of the season is uncultivated and its recognition remains problematic for the whole year. The same is found in the vineyard. Also, corn and wheat are easily confused by the classifier at the beginning of the season. Over time, corn becomes one of the best identified classes along with olive tree and wheat. Again sorghum was revealed to be a crop easy to be identified by the CNN-based classifiers. With respect to 2020, corn is better identified at the end of the season. Using 1D-HH+VV and 3-D, PA of all the classes pass 90% just in June and in August or September 2021

using 1D-VV. The class that earlier exceeds or gets close to PA 90% is sorghum, especially with 1D-VV (already in July) and 3D-HH+VV (already in April).

Using 1D-HH and 1D-VV the highest increment in PA is generally attained in June, whereas using 1D-HH+VV, this increase generally occurs earlier, i.e., in May and in March or April using 3-D. Passing from a classification using backscatter from single polarization to HH+VV with 1-D, especially uncultivated benefited, instead of using 3D-HH+VV, the threshold of PA 70% is reached about a month earlier. Moving from 1-D to 3-D, a noticeable amelioration in PA of all the classes is noticeable especially from March to April.

IV. DISCUSSION

The aim of the project was to demonstrate that *X*-band dual-polarization SAR data can be effectively used to produce an early map of crops in a rural area of central Italy. To fulfill this purpose, we immediately opted for the use of time series of SAR satellite data collected at a high temporal resolution, to avoid the issue of gaps due to cloud cover that often affects optical data [92]. Briefly, priority was given to the temporal regularity of SAR satellite acquisitions over the spectral richness given by optical sensors.

A. Performance and Limitations of the Proposed Method

Being able to benefit from dual-polarization HH and VV, *X*-band, SAR backscatter imagery, like those coming from CSK-PP and a classifier based on CNN, arranged in two different architectures (1-D and 3-D), several tests were carried out on the possible combinations of satellite data acquired in Spring/Summer 2020 and 2021 with classifier configurations for early-season crop classifications.

The use of backscatter from both the polarizations always provided the best classification OA for all the eight monthly time steps (from February till September). When using only one polarization, like for other CSK imaging modes such as StripMap HIMAGE (albeit a much better spatial resolution) and having the choice of selecting imagery among the co-polarized, the VV is preferable. A possible explanation for the best classification performances of backscatter in VV polarization can be its highest sensitivity toward the vertical elements of plants, such as stems or trunks, that often constitute a big percentage of the entire vegetation biomass, as explained in [86] and [93], whereas backscatter in HH polarization is more influenced by soil moisture and roughness [94], which could represent sources of uncertainty for the classifier. The same results have been described in the literature for *X*-band [95] and *C*-band [96], and *L*-band backscatter allows slightly better crop classification results in HH polarization [96], but *L*-band scattering mechanisms on crops are not comparable with those in *X*-band [97]. Regarding the classifier architecture, the 3-D almost always showed better performance with respect to 1-D, except for February 2021, but again the OA of crop classification level marked in this month is very low. The 3-D-based classifiers achieved better performance due to the convolution performed on patches that also consider spatial information. Only the combination

3D-HH+VV permitted to attain the earliest crop classification accuracy above 80% already in April 2020 and in May 2021, and the earliest OA above 90% already in May 2020 and June 2021. Anyway, 90% in OA is always attained from June when using a 3-D classifier, with both single-polarization backscatter and HH+VV (and with 1D-HH+VV).

Based on this two-year-long experiment, the beginning of May, which is equivalent to a total amount of six/seven available images with an average of one/two images per month, emerged as the most likely deadline to achieve an encouraging result of early crop mapping on an agricultural test site with eight/ten classes by means of dual-polarization *X*-band SAR satellite data and CNN technology. In May, the winter species such as fava bean, rapeseed, and wheat are in full vegetation, although they did not reach the peak of growth, whereas the fields that will host the summer species are generally prepared for seeding. The classifier is therefore capable of carrying out a satisfactory classification already when winter species are in the stem elongation phase and the summer species are not sprouted yet and, indeed, these plots are still bare and smooth.

The difference in OA between the same months from two consecutive years of experiment (i.e., May 2020 and May 2021) dramatically decreases after April for 1-D and after March for 3-D for all the configurations of polarization and architecture. Classification OA in May 2020 and 2021 is very close, this is another reason to consider May as the ideal deadline for early classification. Thanks to the adoption of the oversampling algorithm, the negative effect of an unbalanced dataset was strongly reduced since it anticipates the recognition of the less represented classes right away.

The main parameters that play a relevant role in class recognition are the characteristics of the vegetation itself like phenology, structure, density, biomass, and turgor, but its influence on OA falls out of the scope of this research. Anyway, the use of a 3-D classifier and backscatter from both the polarizations tends to mitigate the differences in PA of the classes and among the years, since it copes with the spatial information coming from the 3×3 kernels of convolution and the spectral information coming from both the polarizations. These are other elements suggesting the use of 3D-HH+VV as the best performing approach to use.

The reasons for the weak PA of vineyards in 2020 and 2021 need to be further investigated. A possible explanation may be found in the influence of soil parameters, such as moisture and roughness, that overtake the effect of vegetation in this class.

Indeed in a vineyard, the canopy cover is always incomplete and a large portion of the soil underneath the plants can be targeted by the SAR sensor. Instead, the reason for the weak PA of uncultivated in 2020 and 2021 is due to its high intraclass heterogeneity.

B. Comparison With OA Achieved by Existing Methods

As already stated, an OA close to 99% in crop classification was attained in July using a stack of about ten scenes and 3D-HH+VV in our research. This result is among the best among those obtained in other works in which only SAR data were used for the classification of agricultural areas. For instance, in [35], a maximum OA of 93% is obtained in the recognition of 9 classes using dynamic conditional random fields and a long series of 45 images from Sentinel-1.

In [36], Useya and Chen achieved an OA of 99% using 30 Sentinel-1 scenes and a random forest-based classifier. In [38], Sonobe et al. used a very similar satellite dataset to ours, composed of 16 *X*-band dual-polarization HH and VV scenes to recognize six classes and the highest OA achieved was 95% using a support vector machine. In [37], by using ten *X*-band dual-polarization HH and VV scenes and aiming at recognizing eight classes, Sonobe attained an OA of 92.1% using a multiple kernel learning-based classifier. The results we obtained using only SAR data are good enough to be compared with other studies using optical sensors [69] or the integration/fusion between optical and SAR data [74].

Many published papers referring to "early mapping" of agricultural areas actually confuse this concept with the classification carried out using few images, while a proper early crop mapping is accomplished using the scenes concentrated at the beginning of the crop season. In [89], Kingma and Ba carried out an early mapping exercise of an agricultural area with seven classes using eight scenes from Sentinel-1 attaining OA = 92.9% using an artificial neural network-based classifier. In our experience, OA = 94.9% and OA = 98.5% were achieved, respectively, using seven and nine CSK scenes in 2020 with ten classes. Similar results were achieved using the integration of optical and SAR data like in [90], where OA = 93.7% was reached with the fusion of eight Sentinel-1 and two Landsat-8 images. In [91], Villa et al. used the integration of seven CSK and six Landsat-8 in 2013 and six CSK and eight Landsat-8 scenes in 2014 for the recognition of seven crop classes, attaining results very similar to ours with a decision tree-based classifier. Anyway, the analysis of the marginal gain in terms of OA and PA with the progressive addition of images presented in this article is a novelty, preventive direct quantitative comparison with other publications.

Moving to the comparison of our results with those from other studies related to crop classification using CNN, to the best of our knowledge, the literature seems to lack manuscripts describing the use of SAR satellite data. Although it is very difficult to compare works that aim to map very different test areas, it emerges that external results are in line or outstripped ours when (almost) the same number of classes are foreseen.

For example, in [73], Castro et al. aimed in recognizing 11 classes with 27 Sentinel-1 scenes, obtaining a maximum OA of 71.2%, even if they did not use the entire satellite dataset, but they trained and evaluated a classification approach based on CNN using the stacked features and the reference for the last image in the sequence, respectively. In [71], Adrian et al. aimed in recognizing 13 classes and they attained OA = 58.6% and OA = 81.2% using CNN-2D and CNN-3D, respectively, with a Sentinel-1 dataset.

The results obtained in our work with CNN using only SAR data are also satisfactory even if compared with those achieved through optical and SAR fusion. For example, in [66], Kussul et al. aimed in recognizing 11 classes using 15 Sentinel-1 and 4 Landsat-8 scenes, obtaining an OA of 93.5% with CNN-1D and

94.6 with CNN-2D, respectively. In [72], one of the experiments involved the joint use of Sentinel-1 and Sentinel-2 data and CNN, attaining OA = 87.7% for the recognition of 7 classes and OA = 87.5% for the recognition of 12 classes. Again, in [71], Adrian et al. attained OA = 94.3% with the fusion of Sentinel-1 and Sentinel-2 imagery, in the recognition of 13 classes.

C. Choice of the Metric

We conclude this section by discussing the choice of the metrics. OA is by far the most used metric in the literature for classifier comparison. Other global scores such as the area under the curve, F1-score, Matthews Correlation Coefficient, and Cohen's kappa (K) [98] are less frequently used in multiclass classification problems. They were computed on the proposed experimental results, showing very similar rankings to OA. Since OA is strongly dependent on the dataset balancing [99] we opted to support it with the best and worst PA to provide the reader with a range of performance while preserving a concise statistical description.

V. CONCLUSION

An agricultural test site in the country of central Tuscany, Italy, was selected and two years (2020 and 2021) of *in situ* measurement campaigns were carried out on a regular basis in winter, spring, and summer to gather information on species cultivated on more than one hundred plots each year. Backscatter from dual-polarization HH and VV *X*-band satellite SAR data from the COSMO-SkyMed constellation were acquired from January to September. Backscatter and *in situ* data were used for the training and validation of a crop classifier based on CNN arranged with two different architectures (1-D and 3-D). Ten crop classes in 2020 and eight in 2021, and eight monthly time frames (from February to September) were selected to test the improvement of crop classification over time and the increase of image availability.

Results showed that 3D-CNN structure along with the combination of backscatter at both the polarizations provides the best OA, especially during the first months of the year, i.e., OA is close to 90% in April 2020 and above 80% in May 2021. Nevertheless, the beginning of May, which is equivalent to a total amount of six/seven available images, with an average of 1or 2 images per month, emerged as the most likely deadline for encouraging results of early crop mapping. In case of only single polarization *X*-band data are available, VV is preferable with respect to HH.

Further efforts need to be spent to explain the influence of parameters like phenology, structure, density, biomass, and turgor on classification using *X*-band data and CNN classifier, along with the poor PA marked by vineyard and uncultivated.

ACKNOWLEDGMENT

REFERENCES

[1] FAO, "Sustainable development goals." [Online]. Available: https://www.fao.org/sustainable-development-goals/indicators/241/en/

[2] S. M. Howden, J.-F. Soussana, F. N. Tubiello, N. Chhetri, M. Dunlop, and H. Meinke, "Adapting agriculture to climate change," *Proc. Nat. Acad. Sci. USA*, vol. 104, no. 50, pp. 19691–19696, 2007.

[3] M. D. Nellis, K. P. Price, and D. Rundquist, "Remote sensing of cropland agriculture," in *The SAGE Handbook of Remote Sensing*, vol. 1. Thousand Oaks, CA, USA: Sage, 2009, pp. 368–380.

[4] I. Becker-Reshef, E. Vermote, M. Lindeman, and C. Justice, "A generalized regression-based model for forecasting winter wheat yields in Kansas and Ukraine using MODIS data," *Remote Sens. Environ.*, vol. 114, no. 6, pp. 1312–1323, 2010.

[5] P. Potin, "Sentinel-1 constellation mission operations status," in *Proc. IEEE Int. Geosci. Remote Sens. Symp.*, 2018, pp. 1547–1550, doi: 10.1109/IGARSS.2018.8517743.

[6] The European Space Agency, "The Sentinel missions." [Online]. Available: https://www.esa.int/Applications/Observing_the_Earth/Copernicus/The_Sentinel_missions

[7] The European Space Agency, "Sentinel toolboxes." [Online]. Available: https://sentinel.esa.int/web/sentinel/toolboxes

[8] D. Bargiel, "A new method for crop classification combining time series of radar images and crop phenology information," *Remote Sens. Environ.*, vol. 198, pp. 369–383, 2017.

[9] S. Foerster, K. Kaden, M. Foerster, and S. Itzerott, "Crop type mapping using spectral–temporal profiles and phenological information," *Comput. Electron. Agriculture*, vol. 89, pp. 30–40, 2012.

[10] E. Fiorillo, E. Di Giuseppe, G. Fontanelli, and F. Maselli, "Lowland rice mapping in Sédhiou Region (Senegal) using Sentinel 1 and Sentinel 2 data and random forest," *Remote Sens.*, vol. 12, no. 20, 2020, Art. no. 3403.

[11] D. Stroppiana et al., "In-season early mapping of rice area and flooding dynamics from optical and SAR satellite data," *Eur. J. Remote Sens.*, vol. 52, no. 1, pp. 206–220, 2019.

[12] C. Chen and H. McNairn, "A neural network integrated approach for rice crop monitoring," *Int. J. Remote Sens.*, vol. 27, no. 7, pp. 1367–1393, 2006.

[13] F. Waldner et al., "Land cover and crop type classification along the season based on biophysical variables retrieved from multi-sensor high-resolution time series," *Remote Sens.*, vol. 7, no. 8, pp. 10400–10424, 2015.

[14] L. Zhong, L. Hu, L. Yu, P. Gong, and G. S. Biging, "Automated mapping of soybean and corn using phenology," *ISPRS J. Photogramm. Remote Sens.*, vol. 119, pp. 151–164, 2016.

[15] G. Kite and A. Pietroniro, "Remote sensing applications in hydrological modelling," *Hydrol. Sci. J.*, vol. 41, no. 4, pp. 563–591, 1996.

[16] M. H. Ward, J. R. Nuckols, S. J. Weigel, S. K. Maxwell, K. P. Cantor, and R. S. Miller, "Identifying populations potentially exposed to agricultural pesticides using remote sensing and a geographic information system," *Environ. Health Perspectives*, vol. 108, no. 1, pp. 5–12, 2000.

[17] P. Alexander, M. D. Rounsevell, C. Dislich, J. R. Dodson, K. Engström, and D. Moran, "Drivers for global agricultural land use change: The nexus of diet, population, yield and bioenergy," *Glob. Environ. Change*, vol. 35, pp. 138–147, 2015.

[18] G. Foody, "Fuzzy modelling of vegetation from remotely sensed imagery," *Ecol. Model.*, vol. 85, no. 1, pp. 3–12, 1996.

[19] P. Hao, Y. Zhan, L. Wang, Z. Niu, and M. Shakir, "Feature selection of time series MODIS data for early crop classification using random forest: A case study in Kansas, USA," *Remote Sens.*, vol. 7, no. 5, pp. 5347–5369, 2015.

[20] L. Ranghetti, L. Busetto, A. Crema, M. Fasola, E. Cardarelli, and M. Boschetti, "Testing estimation of water surface in Italian rice district from MODIS satellite data," *Int. J. Appl. Earth Observ. Geoinf.*, vol. 52, pp. 284–295, 2016.

[21] Y. Chen et al., "Mapping croplands, cropping patterns, and crop types using MODIS time-series data," *Int. J. Appl. Earth Observ. Geoinf.*, vol. 69, pp. 133–147, 2018.

[22] L. Li, M. A. Friedl, Q. Xin, J. Gray, Y. Pan, and S. Frolking, "Mapping crop cycles in China using MODIS-EVI time series," *Remote Sens.*, vol. 6, no. 3, pp. 2473–2493, 2014.

[23] D. M. Johnson, "Using the Landsat archive to map crop cover history across the United States," *Remote Sens. Environ.*, vol. 232, 2019, Art. no. 111286.

[24] M. Belgiu and O. Csillik, "Sentinel-2 cropland mapping using pixel-based and object-based time-weighted dynamic time warping analysis," *Remote Sens. Environ.*, vol. 204, pp. 509–523, 2018.

[25] F. Löw, C. Conrad, and U. Michel, "Decision fusion and non-parametric classifiers for land use mapping using multi-temporal RapidEye data," *ISPRS J. Photogramm. Remote Sens.*, vol. 108, pp. 191–204, 2015.

[26] I. L. Castillejo-González et al., "Object-and pixel-based analysis for mapping crops and their agro-environmental associated measures using Quick-Bird imagery," *Comput. Electron. Agriculture*, vol. 68, no. 2, pp. 207–215, 2009.

[27] F. Gao et al., "Toward mapping crop progress at field scales through fusion of Landsat and MODIS imagery," *Remote Sens. Environ.*, vol. 188, pp. 9–25, 2017.

[28] J. Schreier, G. Ghazaryan, and O. Dubovyk, "Crop-specific phenomapping by fusing Landsat and Sentinel data with MODIS time series," *Eur. J. Remote Sens.*, vol. 54, no. sup1, pp. 47–58, 2021.

[29] B. D. Wardlow and S. L. Egbert, "A comparison of MODIS 250-m EVI and NDVI data for crop mapping: A case study for southwest Kansas," *Int. J. Remote Sens.*, vol. 31, no. 3, pp. 805–830, 2010.

[30] D. Arvor, M. Jonathan, M. S. P. Meirelles, V. Dubreuil, and L. Durieux, "Classification of MODIS EVI time series for crop mapping in the state of Mato Grosso, Brazil," *Int. J. Remote Sens.*, vol. 32, no. 22, pp. 7847–7871, 2011.

[31] M. T. Esetlili et al., "Comparison of object and pixel-based classifications for mapping crops using Rapideye imagery: A case study of Menemen Plain, Turkey," *Int. J. Environ. Geoinform.*, vol. 5, no. 2, pp. 231–243, 2018.

[32] Q. Li, C. Wang, B. Zhang, and L. Lu, "Object-based crop classification with Landsat-MODIS enhanced time-series data," *Remote Sens.*, vol. 7, no. 12, pp. 16091–16107, 2015.

[33] H. McNairn, J. Shang, X. Jiao, and C. Champagne, "The contribution of ALOS PALSAR multipolarization and polarimetric data to crop classification," *IEEE Trans. Geosci. Remote Sens.*, vol. 47, no. 12, pp. 3981–3992, Dec. 2009.

[34] Y. Zhang, C. Wang, J. Wu, J. Qi, and W. A. Salas, "Mapping paddy rice with multitemporal ALOS/PALSAR imagery in southeast China," *Int. J. Remote Sens.*, vol. 30, no. 23, pp. 6301–6315, 2009.

[35] B. K. Kenduiywo, D. Bargiel, and U. Soergel, "Crop-type mapping from a sequence of Sentinel 1 images," *Int. J. Remote Sens.*, vol. 39, no. 19, pp. 6383–6404, 2018.

[36] J. Useya and S. Chen, "Exploring the potential of mapping cropping patterns on smallholder scale croplands using Sentinel-1 SAR data," *Chin. Geograph. Sci.*, vol. 29, no. 4, pp. 626–639, 2019.

[37] R. Sonobe, "Parcel-based crop classification using multi-temporal TerraSAR-X dual polarimetric data," *Remote Sens.*, vol. 11, no. 10, 2019, Art. no. 1148.

[38] R. Sonobe, H. Tani, X. Wang, N. Kobayashi, and H. Shimamura, "Discrimination of crop types with TerraSAR-X-derived information," *Phys. Chem. Earth, Parts A/B/C*, vol. 83, pp. 2–13, 2015.

[39] K. Jia, Q. Li, Y. Tian, B. Wu, F. Zhang, and J. Meng, "Crop classification using multi-configuration SAR data in the North China Plain," *Int. J. Remote Sens.*, vol. 33, no. 1, pp. 170–183, 2012.

[40] X. Jiao et al., "Object-oriented crop mapping and monitoring using multi-temporal polarimetric RADARSAT-2 data," *ISPRS J. Photogramm. Remote Sens.*, vol. 96, pp. 38–46, 2014.

[41] D. H. Hoekman and M. A. Vissers, "A new polarimetric classification approach evaluated for agricultural crops," *IEEE Trans. Geosci. Remote Sens.*, vol. 41, no. 12, pp. 2881–2889, Dec. 2003.

[42] C. Hütt and G. Waldhoff, "Multi-data approach for crop classification using multitemporal, dual-polarimetric TerraSAR-X data, and official geodata," *Eur. J. Remote Sens.*, vol. 51, no. 1, pp. 62–74, 2018.

[43] J. M. Lopez-Sanchez, J. D. Ballester-Berman, and I. Hajnsek, "First results of rice monitoring practices in Spain by means of time series of TerraSAR-X dual-pol images," *IEEE J. Sel. Topics Appl. Earth Observ. Remote Sens.*, vol. 4, no. 2, pp. 412–422, Feb. 2010.

[44] S. Paloscia et al., "The sensitivity of COSMO-SkyMed backscatter to agricultural crop type and vegetation parameters," *IEEE J. Sel. Topics Appl. Earth Observ. Remote Sens.*, vol. 7, no. 7, pp. 2856–2868, Jul. 2014.

[45] L. Mascolo, G. Forino, F. Nunziata, G. Pugliano, and M. Migliaccio, "A new methodology for rice area monitoring with COSMO-SkyMed HH–VV PingPong mode SAR data," *IEEE J. Sel. Topics Appl. Earth Observ. Remote Sens.*, vol. 12, no. 4, pp. 1076–1084, Apr. 2019.

[46] R. Devadas, R. Denham, and M. Pringle, "Support vector machine classification of object-based data for crop mapping, using multi-temporal Landsat imagery," *Int. Arch. Photogramm., Remote Sens. Spatial Inf. Sci.*, vol. 39, no. 1, pp. 185–190, 2012.

[47] C. P. Tan, H. T. Ewe, and H. T. Chuah, "Agricultural crop-type classification of multi-polarization SAR images using a hybrid entropy decomposition and support vector machine technique," *Int. J. Remote Sens.*, vol. 32, no. 22, pp. 7057–7071, 2011.

[48] I. Khosravi and S. K. Alavipanah, "A random forest-based framework for crop mapping using temporal, spectral, textural, and polarimetric observations," *Int. J. Remote Sens.*, vol. 40, no. 18, pp. 7221–7251, 2019.

[49] A. O. Ok, O. Akar, and O. Gungor, "Evaluation of random forest method for agricultural crop classification," *Eur. J. Remote Sens.*, vol. 45, no. 1, pp. 421–432, 2012.

[50] N. Kussul, M. Lavreniuk, A. Shelestov, and B. Yailymov, "Along the season crop classification in Ukraine based on time series of optical and SAR images using ensemble of neural network classifiers," in *Proc. IEEE Int. Geosci. Remote Sens. Symp.*, 2016, pp. 7145–7148.

[51] J. Schmidhuber, "Deep learning in neural networks: An overview," *Neural Netw.*, vol. 61, pp. 85–117, Jan. 2015, doi: 10.1016/j.neunet.2014.09.003.

[52] A. Romero, C. Gatta, and G. Camps-Valls, "Unsupervised deep feature extraction for remote sensing image classification," *IEEE Trans. Geosci. Remote Sens.*, vol. 54, no. 3, pp. 1349–1362, Mar. 2015.

[53] M. Gong, H. Yang, and P. Zhang, "Feature learning and change feature classification based on deep learning for ternary change detection in SAR images," *ISPRS J. Photogramm. Remote Sens.*, vol. 129, pp. 212–225, 2017.

[54] Z. Shao and J. Cai, "Remote sensing image fusion with deep convolutional neural network," *IEEE J. Sel. Topics Appl. Earth Observ. Remote Sens.*, vol. 11, no. 5, pp. 1656–1669, May 2018.

[55] M. Kampffmeyer, A.-B. Salberg, and R. Jenssen, "Semantic segmentation of small objects and modeling of uncertainty in urban remote sensing images using deep convolutional neural networks," in *Proc. IEEE Conf. Comput. Vis. Pattern Recognit. Workshops*, 2016, pp. 1–9.

[56] M. Volpi and D. Tuia, "Dense semantic labeling of subdecimeter resolution images with convolutional neural networks," *IEEE Trans. Geosci. Remote Sens.*, vol. 55, no. 2, pp. 881–893, Feb. 2017, doi: 10.1109/TGRS.2016.2616585.

[57] C. Persello and A. Stein, "Deep fully convolutional networks for the detection of informal settlements in VHR images," *IEEE Geosci. Remote Sens. Lett.*, vol. 14, no. 12, pp. 2325–2329, Dec. 2017.

[58] W. Zhao and S. Du, "Spectral–spatial feature extraction for hyperspectral image classification: A dimension reduction and deep learning approach," *IEEE Trans. Geosci. Remote Sens.*, vol. 54, no. 8, pp. 4544–4554, Aug. 2016.

[59] Y. Chen, Z. Lin, X. Zhao, G. Wang, and Y. Gu, "Deep learning-based classification of hyperspectral data," *IEEE J. Sel. Topics Appl. Earth Observ. Remote Sens.*, vol. 7, no. 6, pp. 2094–2107, Jun. 2014.

[60] A. Santara et al., "BASS net: Band-adaptive spectral-spatial feature learning neural network for hyperspectral image classification," *IEEE Trans. Geosci. Remote Sens.*, vol. 55, no. 9, pp. 5293–5301, Sep. 2017.

[61] C. Pelletier, G. I. Webb, and F. Petitjean, "Deep learning for the classification of Sentinel-2 image time series," in *Proc. IEEE Int. Geosci. Remote Sens. Symp.*, 2019, pp. 461–464.

[62] M. Campos-Taberner et al., "Understanding deep learning in land use classification based on Sentinel-2 time series," *Sci. Rep.*, vol. 10, no. 1, pp. 1–12, 2020.

[63] J. Geng, J. Fan, H. Wang, X. Ma, B. Li, and F. Chen, "High-resolution SAR image classification via deep convolutional autoencoders," *IEEE Geosci. Remote Sens. Lett.*, vol. 12, no. 11, pp. 2351–2355, Nov. 2015.

[64] S.-W. Chen and C.-S. Tao, "PolSAR image classification using polarimetric-feature-driven deep convolutional neural network," *IEEE Geosci. Remote Sens. Lett.*, vol. 15, no. 4, pp. 627–631, Apr. 2018.

[65] Y. Zhou, H. Wang, F. Xu, and Y.-Q. Jin, "Polarimetric SAR image classification using deep convolutional neural networks," *IEEE Geosci. Remote Sens. Lett.*, vol. 13, no. 12, pp. 1935–1939, Dec. 2016.

[66] N. Kussul, M. Lavreniuk, S. Skakun, and A. Shelestov, "Deep learning classification of land cover and crop types using remote sensing data," *IEEE Geosci. Remote Sens. Lett.*, vol. 14, no. 5, pp. 778–782, May 2017.

[67] J. Ding, B. Chen, H. Liu, and M. Huang, "Convolutional neural network with data augmentation for SAR target recognition," *IEEE Geosci. Remote Sens. Lett.*, vol. 13, no. 3, pp. 364–368, Mar. 2016, doi: 10.1109/LGRS.2015.2513754.

[68] E. Maggiori, Y. Tarabalka, G. Charpiat, and P. Alliez, "Convolutional neural networks for large-scale remote-sensing image classification," *IEEE Geosci. Remote Sens. Lett.*, vol. 55, no. 2, pp. 645–657, Feb. 2017, doi: 10.1109/TGRS.2016.2612821.

[69] H. Zhao, S. Duan, J. Liu, L. Sun, and L. Reymondin, "Evaluation of five deep learning models for crop type mapping using Sentinel-2 time series images with missing information," *Remote Sens.*, vol. 13, no. 14, Jul. 2021, Art. no. 2790, doi: 10.3390/rs13142790.

[70] Z. Sun, L. Di, H. Fang, and A. Burgess, "Deep learning classification for crop types in North Dakota," *IEEE J. Sel. Topics Appl. Earth Observ. Remote Sens.*, vol. 13, pp. 2200–2213, 2020, doi: 10.1109/JS-TARS.2020.2990104.

[71] J. Adrian, V. Sagan, and M. Maimaitijiang, "Sentinel SAR-optical fusion for crop type mapping using deep learning and Google Earth Engine," *ISPRS J. Photogramm. Remote Sens.*, vol. 175, pp. 215–235, May 2021, doi: 10.1016/j.isprsjprs.2021.02.018.

[72] D. Ienco, R. Interdonato, R. Gaetano, and D. Ho Tong Minh, "Combining Sentinel-1 and Sentinel-2 satellite image time series for land cover mapping via a multi-source deep learning architecture," *IS-PRS J. Photogramm. Remote Sens.*, vol. 158, pp. 11–22, Dec. 2019, doi: 10.1016/j.isprsjprs.2019.09.016.

[73] J. D. B. Castro, R. Q. Feitoza, L. Cue La Rosa, P. M. A. Diaz, and I. D. A. Sanches, "A comparative analysis of deep learning techniques for sub-tropical crop types recognition from multitemporal optical/SAR image sequences," in *Proc. 30th SIBGRAPI Conf. Graph., Patterns Images*, 2017, pp. 382–389, doi: 10.1109/SIBGRAPI.2017.57.

[74] S. Ofori-Ampofo, C. Pelletier, and S. Lang, "Crop type mapping from optical and radar time series using attention-based deep learning," *Remote Sens.*, vol. 13, no. 22, Nov. 2021, Art. no. 4668, doi: 10.3390/rs13224668.

[75] S. Wei, H. Zhang, C. Wang, Y. Wang, and L. Xu, "Multi-temporal SAR data large-scale crop mapping based on U-Net model," *Remote Sens.*, vol. 11, no. 1, Jan. 2019, Art. no. 68, doi: 10.3390/rs11010068.

[76] A. Hirose, *Complex-Valued Neural Networks: Theories and Applications*. Singapore: World Scientific, 2003, doi: 10.1142/5345.

[77] S. Ji, C. Zhang, A. Xu, Y. Shi, and Y. Duan, "3D convolutional neural networks for crop classification with multi-temporal remote sensing images," *Remote Sens.*, vol. 10, no. 2, Jan. 2018, Art. no. 75, doi: 10.3390/rs10010075.

[78] HydroloGIS S.r.l., "SMASH, the free and open source digital field mapping for IOS and android." [Online]. Available: https://www.geopaparazzi.org/smash/

[79] F. Caltagirone et al., "The COSMO-SkyMed dual use Earth Observation Program: Development, qualification, and results of the commissioning of the overall constellation," *IEEE J. Sel. Topics Appl. Earth Observ. Remote Sens.*, vol. 7, no. 7, pp. 2754–2762, Jul. 2014, doi: 10.1109/JS-TARS.2014.2317287.

[80] D. Tapete et al., "Development of algorithms for the estimation of hydrological parameters combining Cosmo-Skymed and sentinel time series with in situ measurements," in *Proc. Mediterranean Middle-East Geosci. Remote Sens. Symp.*, 2020, pp. 53–56, doi: 10.1109/M2GARSS47143.2020.9105313.

[81] E. Meier, U. Frei, and D. Nuesch, "Precise terrain corrected geocoded images, SAR geocoding," in *Data and System*. Heidelberg, Germany: Wichmann Verlag, 1993.

[82] D. Small, F. Holecz, E. Meier, and D. Nuesch, "Absolute radiometric correction in rugged terrain: A plea for integrated radar brightness," in *Proc. IEEE Int. Geosci. Remote Sens. Sens. Manag. Environ.*, 1998, vol. 1, pp. 330–332, doi: 10.1109/IGARSS.1998.702895.

[83] Regione Toscana, "Geoscopio Morfologia." [Online]. Available: http://www502.regione.toscana.it/geoscopio/servizi/wms/MORFOLOGIA.htm

[84] M. Migliaccio, L. Mascolo, F. Nunziata, M. Sarti, and G. Mazzarella, "COSMO-SkyMed HH/VV PingPong mode SAR data to discriminate among Sea, Urban, and Vegetated Areas," *IEEE J. Sel. Topics Appl. Earth Observ. Remote Sens.*, vol. 7, no. 7, pp. 2880–2894, Jul. 2014, doi: 10.1109/JSTARS.2014.2339631.

[85] J. M. Lopez-Sanchez, J. D. Ballester-Berman, and I. Hajnesk, "Rice monitoring in Spain by means of time series of TerraSAR-X dual-pol images," in *Proc. Sci. Appl. SAR Polarimetry Polarimetric Interferometry*, 2009, vol. 668, Art. no. 30.

[86] G. Macelloni, S. Paloscia, P. Pampaloni, F. Marliani, and M. Gai, "The relationship between the backscattering coefficient and the biomass of narrow and broad leaf crops," *IEEE Trans. Geosci. Remote Sens.*, vol. 39, no. 4, pp. 873–884, Apr. 2001.

[87] A. Lapini et al., "Application of deep learning to optical and SAR images for the classification of agricultural areas in Italy," in *Proc. IEEE Int. Geosci. Remote Sens. Symp.*, 2020, pp. 4163–4166, doi: 10.1109/IGARSS39084.2020.9323190.

[88] M. S. Santos, J. P. Soares, P. H. Abreu, H. Araujo, and J. Santos, "Cross-Validation for imbalanced datasets: Avoiding overoptimistic and overfitting approaches [Research Frontier]," *IEEE Comput. Intell. Mag.*, vol. 13, no. 4, pp. 59–76, Nov. 2018, doi: 10.1109/MCI.2018.2866730.

[89] D. P. Kingma and J. Ba, "Adam: A method for stochastic optimization," 2014, *arXiv:1412.6980*.

[90] N. Kussul, L. Mykola, A. Shelestov, and S. Skakun, "Crop inventory at regional scale in Ukraine: Developing in season and end of season crop maps with multi-temporal optical and SAR satellite imagery," *Eur. J. Remote Sens.*, vol. 51, no. 1, pp. 627–636, Jan. 2018, doi: 10.1080/22797254.2018.1454265.

[91] P. Villa, D. Stroppiana, G. Fontanelli, R. Azar, and P. A. Brivio, "In-season mapping of crop type with optical and X-band SAR data: A classification tree approach using synoptic seasonal features," *Remote Sens.*, vol. 7, no. 10, pp. 12859–12886, 2015.

[92] N. Siabi, S. H. Sanaeinejad, and B. Ghahraman, "Effective method for filling gaps in time series of environmental remote sensing data: An example on evapotranspiration and land surface temperature images," *Comput. Electron. Agriculture*, vol. 193, Feb. 2022, Art. no. 106619, doi: 10.1016/j.compag.2021.106619.

[93] G. Fontanelli, S. Paloscia, M. Zribi, and A. Chahbi, "Sensitivity analysis of X-band SAR to wheat and barley leaf area index in the Merguellil Basin," *Remote Sens. Lett.*, vol. 4, no. 11, pp. 1107–1116, Nov. 2013, doi: 10.1080/2150704X.2013.842285.

[94] M. Aubert et al., "Analysis of TerraSAR-X data sensitivity to bare soil moisture, roughness, composition, and soil crust," *Remote Sens. Environ.*, vol. 115, no. 8, pp. 1801–1810, Aug. 2011, doi: 10.1016/j.rse.2011.02.021.

[95] D. Bargiel and S. Herrmann, "Multi-temporal land-cover classification of agricultural areas in two European regions with high resolution spotlight TerraSAR-X data," *Remote Sens.*, vol. 3, no. 5, pp. 859–877, Apr. 2011, doi: 10.3390/rs3050859.

[96] H. Skriver, "Crop classification by multitemporal C- and L-band single- and dual-polarization and fully polarimetric SAR," *IEEE Trans. Geosci. Remote Sens.*, vol. 50, no. 6, pp. 2138–2149, Jun. 2012, doi: 10.1109/TGRS.2011.2172994.

[97] N. Baghdadi, N. Boyer, P. Todoroff, M. El Hajj, and A. Bégué, "Potential of SAR sensors TerraSAR-X, ASAR/ENVISAT and PALSAR/ALOS for monitoring sugarcane crops on Reunion Island," *Remote Sens. Environ.*, vol. 113, no. 8, pp. 1724–1738, Aug. 2009, doi: 10.1016/j.rse.2009.04.005.

[98] M. Grandini, E. Bagli, and G. Visani, "Metrics for multi-class classification: An overview," 2020, *arXiv:2008.05756*.

[99] Y. Sun, A. K. C. Wong, and M. S. Kamel, "Classification of imbalanced data: A review," *Int. J. Pattern Recognit. Artif. Intell.*, vol. 23, no. 4, pp. 687–719, Jun. 2009, doi: 10.1142/S0218001409007326.

Giacomo Fontanelli received the B.Sc. and M.Sc. degrees in forest and environmental science from the University of Florence, Florence, Italy, in 2007, and the Ph.D. degree in methods and technologies for environmental monitoring from the University of Basilicata, Potenza, Italy, in 2014.

He joined the Institute of Applied Physics of the National Research Council (IFAC-CNR), Florence, in 2010. He moved to the Institute for Electromagnetic Sensing of the Environment (IREA-CNR), Milan, Italy, in 2013. From 2016 to 2018, he was an Agro-Environmental Scientist with Rothamsted Research, Harpenden, U.K., before coming back to IFAC-CNR, in 2018, where he is currently a Researcher. He worked on many national and international projects, funded by ESA, ASI, EC, and Innovate U.K. His research interests include the identification of indices from satellite remotely sensed data to describe forest status and crop growth and productivity, and he is also focused on providing useful information to farmers using satellite data, to help them in agricultural practices and decision making.
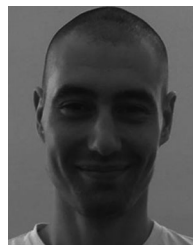
Alessandro Lapini received the M.Sc. degree (*summa cum laude*) in telecommunications engineering and the Ph.D. degree in computer science, systems, and telecommunications from the University of Florence, Florence, Italy, in 2010 and 2014, respectively.

Since 2014, he has been a Research Assistant with the University of Florence, where he was initially with the Department of Information Engineering and then with the Department of Industrial Engineering since 2015. From 2016 to 2018, he was a Research Fellow with the Department of Industrial Engineering, University of Florence. Since 2019, he is with the Microwave Remote Sensing Group, Institute of Applied Physics Nello Carrara, Consiglio Nazionale delle Ricerche, Florence. His research interests include signal and image processing, particularly in the field of remote sensing and biomedical imaging, acoustics, and active noise control.

Leonardo Santurri was born in Florence, Italy, in 1964. He received the M.S. (*cum laude*) in electronic engineering and the Ph.D. degree in information technology and society from the University of Florence, Florence, Italy, in 1998 and 2005, respectively.

In 1999, he attended the Course of Specialization and Advanced Training in the University of Florence. Since 2001, he has been a researcher with the Institute of Applied Physics (IFAC) "Nello Carrara" of Italian National Research Council (CNR), Florence, Italy. He has been involved in international research projects funded by the European and Italian Space Agency on remote sensing topics and has authored or coauthored 10 papers in peer-reviewed journals and books and a total of nearly 50 international publications. His research interests include the processing of data acquired by satellite platforms and remote sensing data applications.

Simone Pettinato (Member, IEEE) was born in Florence, Italy, in 1972. He received the M.S. degree in telecommunications engineering from the University of Florence, Florence, Italy, in 2002, and the Ph.D. degree in "methods and technologies for environmental monitoring" from the University of Basilicata, Potenza, Italy, in 2007.

Since 2003, he has been a Scientist with the Microwave Remote Sensing Group, Institute of Applied Physics of the National Research Council (IFAC-CNR). At the end of 2013, he got the permanent position. The objective of his research consists mainly of the investigation of the natural surfaces using active and passive microwave sensors to retrieve information on geophysical parameters related to the hydrological cycle (soil moisture, snow, and vegetation). He participated, as a coinvestigator, in different national and international scientific projects funded by the European Community (FLOODMAN, ENVISNOW) and European Space Agency (GRASS, LEIMON, CORE-H2O, DOMEX-2, DOMEX-3, GPS-SIDS, GNSS-BIO). In 2009, 2010, and 2012, he was involved in three Antarctic expeditions to allow the execution of the DOMEX-2, DOMEX-3, and GPS-SIDS projects. He was involved in Italian Space Agency (ASI) projects for floods forecast (PROSA: Satellite Observation Products for Meteorological Alert), Cosmo-SkyMed applications (Hydro-Cosmo: the retrieval and monitoring of Land Hydrological parameters for Risk and Water Resources Management), CATARSI (Cap and Trade Assessment by Remote Sensing Investigation) and SIASGE (Definition of products at X and X+L bands for SIASGE support). He is a coinvestigator in a regional project (Hydrocontroller) for the monitoring of hydrologic risk, and in an international project for sustainable water management for the economic growth and sustainability of the Mediterranean region (OPTIMED-WATER) in the frame of FP7 of the European Union. He is also involved in the ASI project METEMW that aims to develop innovative algorithms for the retrieval of hydrological parameters. He is the author or coauthor of 100 papers published in international peer-reviewed journals and conference proceedings.

Emanuele Santi (Senior Member, IEEE) received the M.S. degree in electronic engineering from the University of Florence, Florence, Italy, in 1997, and the Ph.D. degree in Earth's remote-sensing techniques from the University of Basilicata, Potenza, Italy, in 2005.

Since 1998, he has been a Researcher with the Microwave Remote Sensing Group, Institute of Applied Physics, National Research Council, Florence. He was and is currently involved in many national and international projects funded by the Italian Space Agency (ASI), European Community, European Space Agency, and Japanese Aerospace Exploration Agency, acting as a Team Leader, a WP Leader, and a coinvestigator. He authored or coauthored 168 articles, published in ISI journals, books, and conference proceedings (source Scopus). His research interests include the development and validation of models and inversion algorithms based on machine learning for estimating the geophysical parameters of soil, sea, snow, and vegetation from microwave emission and scattering.

Dr. Santi is a member of the "Centro di Telerilevamento a Microonde" (Microwave Remote Sensing Center), the Vice-Chair of the IEEE GRS Chapter CNI-29, and Conference Chair of the SPIE Europe Remote Sensing conference RS-106. In 2020, he was the Chair of the 16th Symposium on Microwave Radiometry MicroRad. In 2018, he was the recipient of the IEEE GRSS J-STARS Prize Paper Award for the best paper published in the J-STARS journal in 2017.

Giuliano Ramat (Member, IEEE) received the B.Sc. and M.Sc. degrees in forest and environmental science from the University of Florence, Florence, Italy, in 1997.

He joined the Italian Agency for Development Cooperation in 2000 as training staff in the Master on Geomatics and Natural Resources Evaluation. He was a Remote Sensing and GIS Key Expert in several international projects for development cooperation, mainly in Algeria (2005–2010) and Afghanistan (2014–2018) and also in South America, East and Sub Saharan Africa. He has been a Remote Sensing trainer and a GIS trainer both in the frame of University Masters and over e-learning platforms. In 2018, he moved to the Social Geography Lab, Florence University, and in 2019, joined the Institute of Applied Physics of the National Research Council (IFAC-CNR). He is interested in the integrations of open source GIS, field data collection, and remote sensing techniques, in arid and semiarid environments, to produce the land cover and land cover change maps mainly focused on rangelands and natural vegetation.

Simone Pilia (Senior Member, IEEE) is currently working toward the Ph.D. degree in monitoring physiological crop stress status by using remotely sensed data with the University of Basilicata, Potenza, Italy.

In particular, currently, his studies focus on the retrieval of natural parameters, in detail for snow soil and vegetation, by microwave emission and scattering. Since 2018, he has been with National Research Council (CNR). His research interests include microwave applications such as antenna design and microwave remote sensing.

Fabrizio Baroni received the M.S. and Ph.D. degrees in physics from the University of Florence, Italy in 2002 and 2007, respectively.

He won the Giampietro Puppi Award for doctoral thesis in physics and astrophysics in 2009. In the past he was active in quantum mechanics, statistical mechanics and teaching. Currently, he is with the Microwave Remote Sensing Group, Institute of Applied Physics "Nello Carrara" (IFAC), National Research Council (CNR), Florence. His research interests are in modelling of snowpack, soil and vegetation and application to retrieval of physical parameters by active and passive microwave remote sensing. He is referee for some international journals.

Deodato Tapete received the B.Sc. degree (*cum laude*) in mathematics, physics, and natural sciences from the University of Florence, Florence, Italy, in 2005, the M.Sc. degree (*cum laude*) in mathematics, physics, and natural sciences from the University of Bologna, Bologna, Italy, in 2005 and 2007, respectively, and the Ph.D. degree in Earth sciences from the University of Florence, in 2012.

He is currently a researcher in Earth observation and data analytics with the Italian Space Agency (ASI), Rome, Italy, a Principal Investigator of research projects, and a Project Manager of funding contracts with Public Research Bodies and Small Medium Enterprises aimed at developing, testing, and prototyping of SAR image processing algorithms and derived products. He is involved in the Committee on Earth Observation Satellites and research collaborations in the fields of natural hazards, disaster risk reduction, urban remote sensing, archaeology, and cultural heritage.

Francesca Cigna received the B.Sc. and M.Sc. degrees (*cum laude*) in environmental engineering from the University of Palermo, Palermo, Italy, in 2006 and 2007, respectively, and the Ph.D. degree in Earth sciences from the University of Florence, Florence, Italy, in 2011.

Since 2021, she has been a Senior Researcher in Earth observation with the Institute of Atmospheric Sciences and Climate of the National Research Council (ISAC-CNR), Rome, Italy. She was with the Italian Space Agency (ASI), the British Geological Survey of the Natural Environment Research Council, and the University of Florence. Her research interests include satellite SAR and optical imagery, advanced InSAR and change detection methods, mapping and monitoring of natural and anthropogenic hazards and risks in urban and rural environments, shallow geological processes, land subsidence, hydrogeology, landscape archaeology, and cultural heritage.

Simonetta Paloscia (Fellow, IEEE) received the M.S. degree in agricultural sciences from the University of Florence, Florence, Italy, in 1979.

She has been with the National Research Council (CNR), since 1984. Since 2004, she has been the scientific responsible for the Microwave Remote Sensing Group, Institute of Applied Physics of the National Research Council (IFAC-CNR), and the research line "Microwave remote sensing of natural surfaces," in the EO Project of CNR. Since 1996, she has been a Principal Investigator in the JAXA Science Team of AQUA/AMSR-E and GCOM/AMSR-2 for algorithms development of soil moisture and vegetation biomass retrieval. In 2010, she was nominated the Head of Research with the National Research Council. She was PI and Co-I of many national and international projects (ASI, EC, ESA, and JAXA). She is member of the SMAP JPL/NASA Science Team. She was a member of organizing and steering committees of international meetings (Specialist Meeting on Microwave Radiometry and IGARSS). She is a member of the permanent Steering Committee of MicroRad Meeting. She was General Co-Chair of the MicroRad 1999 and 2008, and URSI-F 2010 meetings organized in Florence. She is the author and coauthor of more than 100 works published in international journals and books, of more than 200 papers published on proceedings of international meetings. Her current research focuses on the study of microwave emission and scattering of soil (bare and snow-covered) and vegetation.

Ms. Paloscia has been a URSI Fellow since 2020. She was the Vice-Chair and the Chair of URSI Commission F from 2011 to 2017. She is currently an Associate Editor for the *International Journal of Remote Sensing*, IEEE JOURNAL OF SELECTED TOPICS IN APPLIED EARTH OBSERVATIONS AND REMOTE SENSING, and *European Journal of Remote Sensing*. From 1994 to 2010, she had a temporary teaching contract of "Microwave Remote Sensing Applications" for the Professional Master "Geomatics and Natural Resources Evaluation" with the "Istituto Agronomico per l'Oltremare" of the Ministry of Foreign Affairs in Florence.